

WEAK LENSING SURVEYS AND THE INTRINSIC CORRELATION OF GALAXY ELLIPTICITIES

RUPERT A.C. CROFT AND CHRISTOPHER A. METZLER

Harvard-Smithsonian Center for Astrophysics, Cambridge, MA 02138

Draft version December 6, 2018

ABSTRACT

We explore the possibility that an intrinsic correlation between galaxy ellipticities arising during the galaxy formation process may account for part of the shear signal recently reported by several groups engaged in weak gravitational lensing surveys. Using high resolution N-body simulations we measure the projected ellipticities of dark matter halos and their correlations as a function of pair separation. With this simplifying, but not necessarily realistic assumption (halo shapes as a proxy for galaxy shapes), we find a positive detection of correlations up to scales of at least $20 h^{-1}\text{Mpc}$ (limited by the box size). The signal is not strongly affected by variations in the halo finding technique, or by the resolution of the simulations (over the range tested). We translate our three dimensional results into angular measurements of ellipticity correlation functions and shear variance which can be directly compared to observational results. We also make simulated angular surveys by projecting our simulation boxes onto the plane of the sky and applying a radial selection function. Measurements from these catalogs are consistent with the analytic projection of the statistics. Interestingly, the shear variance we measure is a small, but not entirely negligible fraction (from $\sim 10 - 20\%$, depending on the angular scale) of that seen by the observational groups, and the ellipticity correlation functions approximately mimic the functional form expected to be caused by weak lensing. The amplitude of these projected quantities depends strongly on the width in redshift of the galaxy distribution. If in the future photometric redshifts are used to pick out a screen of background galaxies with a small redshift width, then the intrinsic correlation may become comparable to the weak lensing signal. Although we are dealing with simulated dark matter halos, we might expect there to be a similar sort of signal when real galaxies are used. This could be checked fruitfully using a nearby sample with known redshifts.

Subject headings: Cosmology: theory – large scale structure of Universe

1. INTRODUCTION

The large-scale mass distribution in the Universe is expected, through gravitational lensing, to imprint itself on the pattern of ellipticities measured from background galaxies (e.g., Blandford et al. 1991; Miralda-Escudé 1991). The angular correlations of such ellipticities, or the variance in ellipticities averaged in angular cells (amongst other statistics) can be compared to expectations for different cosmological models, and in principle can discriminate between them (e.g., Blandford et al. 1991; Miralda-Escudé 1991; Kaiser 1992; Jain & Seljak 1997). Since lensing is induced by the foreground mass distribution only, it provides the most direct method of studying the structure of mass in the Universe on large scales. Accordingly, detecting the shear signal induced by large scale structure has been the subject of a great deal of observational effort. Recently, four separate groups have reported detections of this cosmic shear, at levels comparable to that expected from currently popular models of structure formation (Van Waerbeke et al. 2000 [hereafter VW]; Bacon, Refregier & Ellis 2000; Wittman et al. 2000; Kaiser, Wilson & Luppino 2000 [hereafter KWL]).

In attributing the observed correlations of ellipticities, or the shear variance, to large-scale structure, an important assumption is that the sample of background galaxies used contains no intrinsic correlation of ellipticities. If such a correlation were present in the sample of lensed sources, it could be attributed to lensing, and may enhance the detected signal. The argument for discounting this possibility is that a pair of galaxies separated by a small dis-

tance on the sky are nonetheless on average separated by a large distance along the line of sight. If a particular pair of galaxies are separated by a large distance, there is no good theoretical reason to expect their ellipticities to be intrinsically correlated.

However, the angular correlation of ellipticities predicted to be due to lensing is quite small — on the order of 10^{-4} out to scales of several arcminutes. To detect this correlation against the random variations of galaxy ellipticities, observers take deep images and use large samples of background galaxies, perhaps 10^5 per square degree. Some of these galaxies can be expected to be close not only in projection, but in real space as well. To what degree should we expect correlations in the actual ellipticities of nearby galaxies, and how much would the projection of such correlations add to any observed lensing signal?

That such intrinsic correlations in galaxy ellipticities may exist is not implausible. If elongation by local tidal fields contributed significantly to galaxy ellipticities, then nearby galaxies could be expected to sample the tidal field in the same fashion, producing similar elongations. Alternately, if some elongation originating from a galaxy's last merger were to survive for a time comparable to the characteristic merger timescale for its environment, then one might expect galaxies to be preferentially aligned along the local large-scale structure, and thus similarly to each other. On larger scales, such elongation in cosmic structures appears to be present. For instance, the effects of large scale structure on the shapes of galaxy clusters have been the subject of much study. Cosmological N-body

simulations have suggested that clusters tend to be oriented towards neighboring clusters or in directions defined by adjoining filaments and the merging subclusters which drain along them. (Dekel, West & Aarseth 1984; West, Dekel & Oemler 1989; West, Villumsen & Dekel 1991; van Haarlem & van de Weygaert 1993; Splinter et al. 1997; de Theije, van Kampen & Slijkhuis 1998). Observations have typically indicated the presence of such alignments, either towards nearby clusters (Binggeli 1982; Flin 1987; West 1989a,b; Rhee, van Haarlem & Katgert 1992; Plionis 1994) or towards nearby large-scale structure in the galaxy distribution (Argyres et al. 1986; Lambas, Groth & Peebles 1988); although not all studies support the presence of such alignments (Struble & Peebles 1985; Ulmer, McMillan & Kowalski 1989; Fong, Stevenson & Shanks 1990). The existence of correlations in the alignment of large-scale structures appears quite possible; perhaps similar intrinsic correlations in alignment exist on galactic scales.

Theoretical expectations for the degree of correlation of intrinsic ellipticities can in principle be derived. The local gravitational shear can be expected to either align the intrinsic angular momentum of nearby galaxies (Lee & Pen 2000), or to similarly deform neighboring, non-rotating galaxies through tidal distortion (Ciotti & Dutta 1994). Thus, the statistics of the local tidal field can be related to the statistics of galaxy angular momenta (Catelan & Theuns 1996a,b; Catelan & Theuns 1997; Sugerman, Summers & Kamionkowski 1999); and therefore to the intrinsic correlations in galaxy ellipticities (Coutts 1996; Lee & Pen 2000; Catelan et al. 2000, in preparation; Mackey and White 2000, in preparation).

There have been numerous attempts to detect intrinsic correlations in galaxy alignments using low redshift samples; the picture painted by this work is unclear, as we can see from the following sample. Flin (1988) considered a sample of 118 galaxies in the Perseus supercluster and found that the spin axes of these galaxies were aligned with the supercluster plane. Muriel & Lambas (1992) reported a correlation of alignments seen with spirals taken from the ESO catalog and analyzed in three dimensions; when only projected data was considered, the correlation was no longer present. Garrido et al. (1993) analyzed a sample covering a large area of sky in the northern hemisphere and claimed to find no evidence for correlations in alignment except within the Coma supercluster. Han, Gould & Sackett (1995) examined the spins of 60 galaxies in the Ursa Major filament and found no evidence for any alignment of spins. Cabanela & Aldering (1998) considered galaxy shapes extracted from a survey of Perseus-Pisces conducted using an automated plate scanner; statistically significant and color dependent correlations of galaxy ellipticities were found. On the other hand, Cabanela & Dickey (1999) used HI observations to determine the spins of 54 galaxies in the Perseus-Pisces supercluster; and found no evidence for preferential alignments of spin vectors. At this time evidence favors an orientation alignment between cD galaxies and the major axis of their parent cluster; but the presence or absence of any other galaxy shape correlations remains undetermined.

In this paper, we use Nbody simulations to make theoretical predictions for the correlation of intrinsic galaxy ellipticities. For simplicity, we work with directly with the projected ellipticities of the simulated dark matter halos,

without making assuming any model for the way galaxies form within them. The significance of our results will therefore be entirely dependent on whether galaxy ellipticities behave significantly differently from their halos, a problem we leave to future gasdynamical simulations.

The layout of the paper is as follows. In §2, we describe the N-body dataset used, our halo catalog, and our measurement of projected ellipticities from the halos. We measure the three dimensional correlation functions of projected ellipticities in §3, and in §4 we describe the construction of simulated surveys from our halo catalogs, with a geometry designed to mimic weak lensing observations. In §5, we project the three dimensional correlation functions into angular statistics, including the shear variance. We also compute these angular measures directly from our simulated surveys (as a consistency check). We compare our results to current observational data in §6, before discussing and summarizing our results in §7.

2. SIMULATED HALOS

2.1. *Nbody simulations*

Our requirements are that the simulation volume be large enough to capture the large scale tidal field that may cause correlations to arise between halo shapes, while at the same time having enough mass resolution to follow the formation of galaxy sized halos with a reasonable number of particles. We use outputs from Nbody simulations run by the Virgo Consortium (see e.g., the author list of Jenkins et al. 1998 for Virgo members) and which they have generously made public. The simulations are part of a set of different models, although we only use one here, the currently favoured cosmological constant-dominated cold dark matter (Λ CDM) model. The parameters of this model are as follows, $\Omega_m = 0.3$ (the matter density at $z = 0$), $\Omega_\Lambda = 0.7$ (the contribution of Λ to the critical density at $z=0$), $\Gamma = 0.21$, which is the shape parameter of the initial power spectrum. The normalization was set so that $\sigma_8 = 0.9$, (the rms matter fluctuations in $8 h^{-1}$ Mpc spheres extrapolated to $z = 0$).

We use two different simulations, one run with a box size of $141.3 h^{-1}$ Mpc, and another in a box of size $240 h^{-1}$ Mpc, both with 256^3 particles. The mass per particle in the former case is $1.4 \times 10^{10} h^{-1} M_\odot$, and in the second it is 5 times larger. The Nbody code used was an adaptive particle-particle particle-mesh code (Couchman, Thomas and Pearce), and the gravitational softening length was $30 h^{-1}$ kpc (for the smaller box). For more details, the reader is referred to the Virgo papers, including Kauffmann et al. (1999) for the smaller box simulation. Unless stated otherwise, all our analysis will be carried out using the higher resolution simulation, with the other being used as a check of the effects of lower resolution. We use only the $z = 1$ output in each case, as we will be interested in comparing to lensing observations where the peak of the galaxy distribution is expected to lie close to this redshift.

2.2. *Halo finding*

Our analysis will be restricted to dark matter halos, and we will make no attempt to identify luminous galaxies in the simulations. In order to keep interpretation of our results simple, we will focus mostly on halos picked from the particle distribution using one easy to use groupfinder,

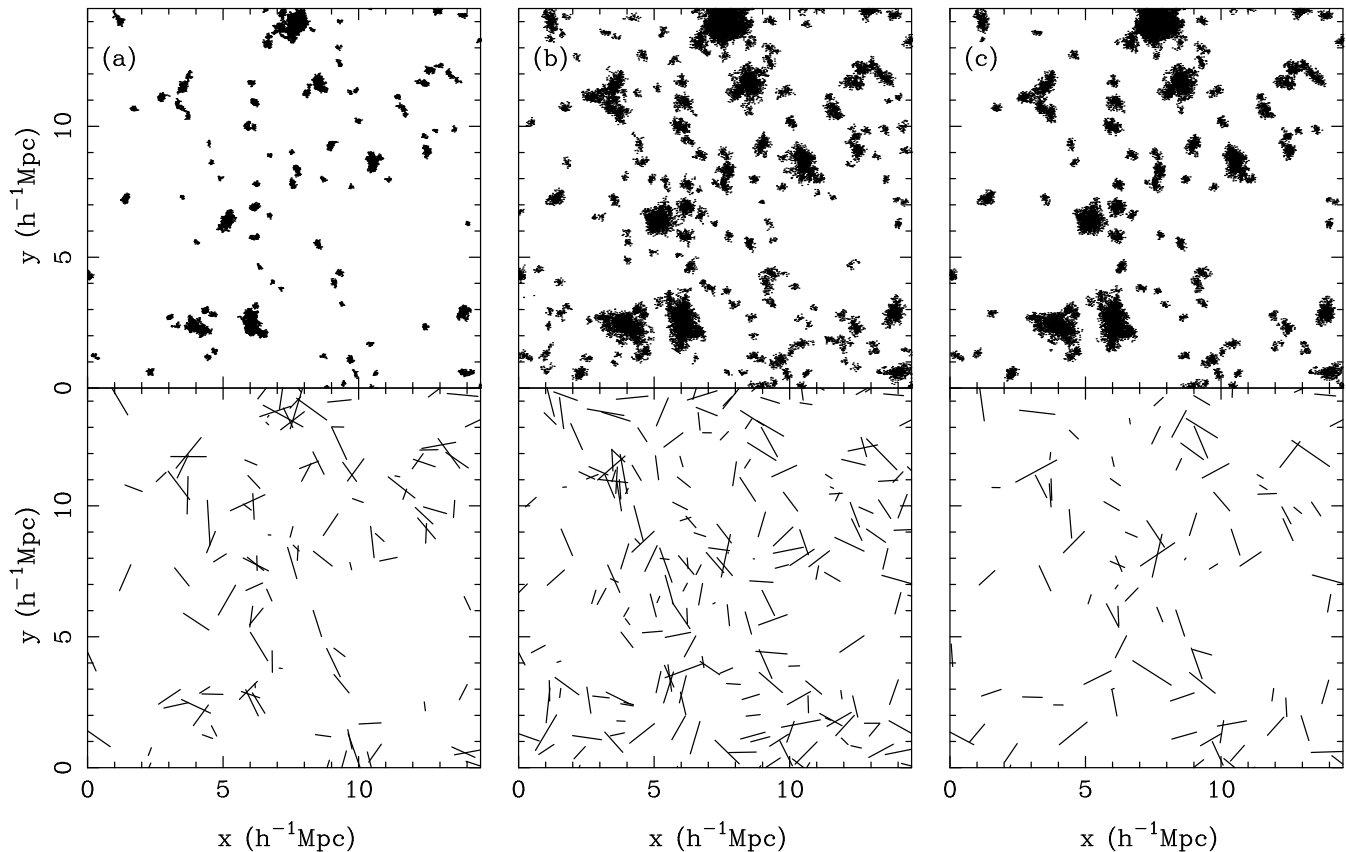


FIG. 1.— The (x,y) positions of particles which fall in halos (upper panels). We plot particles found in a portion of the simulation box of (z) depth $40 h^{-1}\text{Mpc}$. Three different group finding techniques were used: (a) friends-of-friends with a linking length of 0.1 times the mean interparticle separation ($\text{FOF}_{0.1}$), (b) friends-of-friends with a linking length of 0.2 times the mean interparticle separation ($\text{FOF}_{0.2}$), and (c) the HOP groupfinder. In the lower panels, we show the x and y components of the ellipticity of each halo (see text). The scale is such that an ellipticity of 1 corresponds to a bar of length $2 h^{-1}\text{Mpc}$.

the friends-of-friends (FOF) algorithm (e.g., Davis et al. 1985). A quick comparison will also be made with results from the publically available HOP groupfinding code (Eisenstein and Hut 1998).

In FOF, the one free parameter is the linking length as a fraction of the mean interparticle separation, b . This in a crude way governs the overdensity at the edge of the halo. We present some results using either $b = 0.1$, or $b = 0.2$. The latter is often used so that particles will be chosen from regions roughly inside the virial overdensity threshold of halos. With the former we will be picking out the denser (by approximately a factor of 8) central parts of halos.

The HOP groupfinder works in a different way, using a smoothed overdensity field calculated at the positions of the particles. A group merging stage places subgroups together which fall inside a certain density contrast. The HOP algorithm has 6 free parameters; in this paper we use the fiducial values recommended by Eisenstein and Hut (1998).

In Figure 1, we plot the particles which ended up inside halos for each of the three groupfinding choices ($\text{FOF}_{0.1}$, $\text{FOF}_{0.2}$, and HOP). Only a small fraction of the box is shown, centred on an overdense region (the density inside the volume plotted, which measures $15 \times 15 \times 40 h^3\text{Mpc}^{-3}$ is 1.6 times the cosmic mean). A lower mass cut of 20 particles ($2.8 \times 10^{11} h^{-1} M_{\odot}$) has been applied to the halo list, which results in there being 20569 $\text{FOF}_{0.1}$ halos in the

whole simulation volume, 42024 $\text{FOF}_{0.2}$ halos, and 18023 HOP halos. Of course, the $\text{FOF}_{0.1}$ halos will tend to coincide with the central regions of the other halos, so that if we define the total mass of a halo to be its virial mass, then this will be larger for the $\text{FOF}_{0.1}$ objects than the number of particles which we plot in Fig 1. The $\text{FOF}_{0.1}$ halos are interesting because they will offer a good check of the robustness of our results, when we ask below whether the ellipticities of the dense central regions are correlated in the same way as the outer parts of the halos.

2.3. Halo ellipticities

Although it is possible to measure three dimensional ellipticities for halos, we will work here only with quantities which are projected onto the plane of the sky, for ease of comparison with observational data.

We estimate the ellipticity components of each halo by measuring the second moments of the projected mass distribution in a way analogous to that used for the surface brightness distribution of galaxies (Valdes et al. 1983, Miralda-Escudé 1991):

$$e_1 = \frac{I_{xx} - I_{yy}}{I_{xx} + I_{yy}}, \quad e_2 = \frac{2I_{xy}}{I_{xx} + I_{yy}}, \quad (1)$$

where

$$I_{xx} = \frac{\sum_{i=1}^N (x_i - \bar{x})^2}{N}, \quad I_{yy} = \frac{\sum_{i=1}^N (y_i - \bar{y})^2}{N}, \quad (2)$$

and

$$I_{xy} = \frac{\sum_{i=1}^N (x_i - \bar{x})(y_i - \bar{y})}{N}. \quad (3)$$

Here, \bar{x} and \bar{y} are the coordinates of the center of mass of the halo in question, which contains N particles of equal mass. In the observational case, these moments are often calculated using the surface brightness weighted by a function chosen to maximize the S/N of the measurement (see e.g., VW). In our case, as we have mentioned above, we will probe the sensitivity of our measurements to variations of this sort by comparing halos chosen with a large FOF linking length to those using a small value which effectively give a non-zero weight only to the dense central regions.

When working with pairwise statistics, such as the ellipticity correlation function (see §3), it will be advantageous to redefine e_1 and e_2 for each pair of halos, with the x -axis defined to be line joining the halo centres and the y -axis a line perpendicular to it.

The quantity (e_1, e_2) defines a pseudovector, of length $e = \sqrt{e_1^2 + e_2^2}$. A positive e_1 component indicates a stretching along the x -axis, and a negative component a stretching along the y -axis. The e_2 component is likewise a measure of the stretching along axes at 45 deg to the x and y axes. If we have an ellipse of ellipticity e ($e \equiv (1 - q^2)/(1 + q^2)$, where q is the ratio of minor and major axis lengths), then

$$e_1 = e \cos(2\beta), \quad e_2 = e \sin(2\beta), \quad (4)$$

where β is the angle between the major axis and the x -axis.

In the bottom three panels of Fig. 1, we plot the ellipticities of the halos chosen by the three groupfinders. For each halo, we show a bar with length proportional to e , oriented along the direction of the major axis. It is difficult to pick out by eye any tendency for halos to be aligned. One worry which we might have had concerns the tendency of close halos to be joined together by thin “necks” of particles and for the groupfinder to count such pairs as one halo. If these halos are distributed along filaments, then we might expect an artificial alignment to arise. This does not seem to be an obvious problem here. For example, if we look at halos picked out by the FOF_{0.1} and FOF_{0.2} groupfinders, the ellipticities and directions appear to be fairly similar even though different parts of the halo are being used to calculate them. We will check the statistical tendencies for alignments in the next section. The HOP halos do in several cases appear to be made from several small halos joined together. Presumably this could be alleviated by tuning the free parameters which govern the method, but we have not attempted to do this.

In Fig. 2, we show the probability distribution of e values for the halos (again with > 20 member particles) picked out by the three groupfinders. They are all fairly similar, with a mean e around 0.4, slightly higher than the 0.3 typical of real galaxies (e.g., Wittman et al. 2000).

3. ELLIPTICITY CORRELATIONS IN THREE DIMENSIONS

Observationally, ellipticity correlations are measured as a function of angular separation, on the plane of the sky (at least for weak lensing surveys). With distance information (for example, using redshifts), it would be possible to measure them as a function of separation in three dimensions, and this is what it is most natural to do using our Nbody simulations. In this section, we will do this, and later convert the measurements to angular correlations which can be compared to weak lensing survey results. This conversion will be done in two different ways. The first is an analytical projection of our three dimensional results using Limber’s equation (Limber, 1959). The second is a direct measurement from simulated surveys made by projecting the halo distributions in the box, and applying a radial selection function. In the present section, although we will be dealing with halo separations in three dimensions, it is worth bearing in mind that we restrict ourselves to quantities which can be measured directly observationally (albeit with redshifts), so that the ellipticities we will be correlating are projected ellipticities (defined in Equation 1).

Two ellipticity correlations can be defined (following Miralda-Escudé 1991) as

$$c_{11}(r) = \langle e_1(\mathbf{x})e_1(\mathbf{x} + \mathbf{r}) \rangle, \quad (5)$$

and

$$c_{22}(r) = \langle e_2(\mathbf{x})e_2(\mathbf{x} + \mathbf{r}) \rangle, \quad (6)$$

together with a cross-correlation,

$$c_{12}(r) = \langle e_1(\mathbf{x})e_2(\mathbf{x} + \mathbf{r}) \rangle, \quad (7)$$

where \mathbf{r} is the three dimensional vector of length r joining each pair of halos. Here we have defined the ellipticity components, e_1 and e_2 with respect to axes which are the projection into the $x - y$ plane of the line joining each pair of halos and a line orthogonal to it which lies also in the x - y plane.

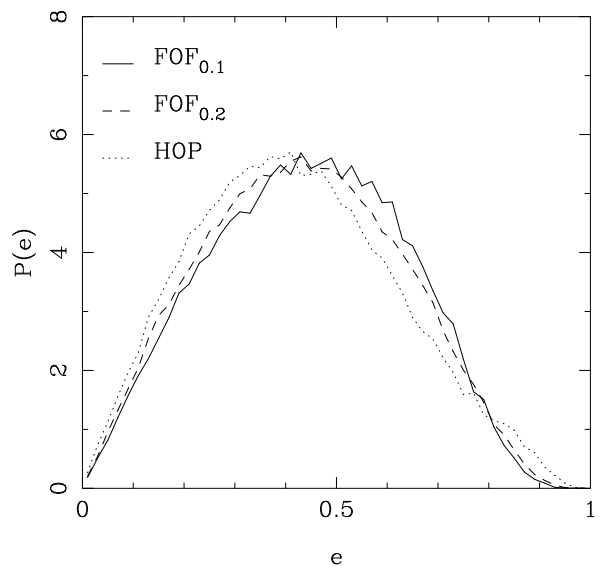


FIG. 2.— The probability distribution function of halo ellipticities, for the 3 different group finding techniques.

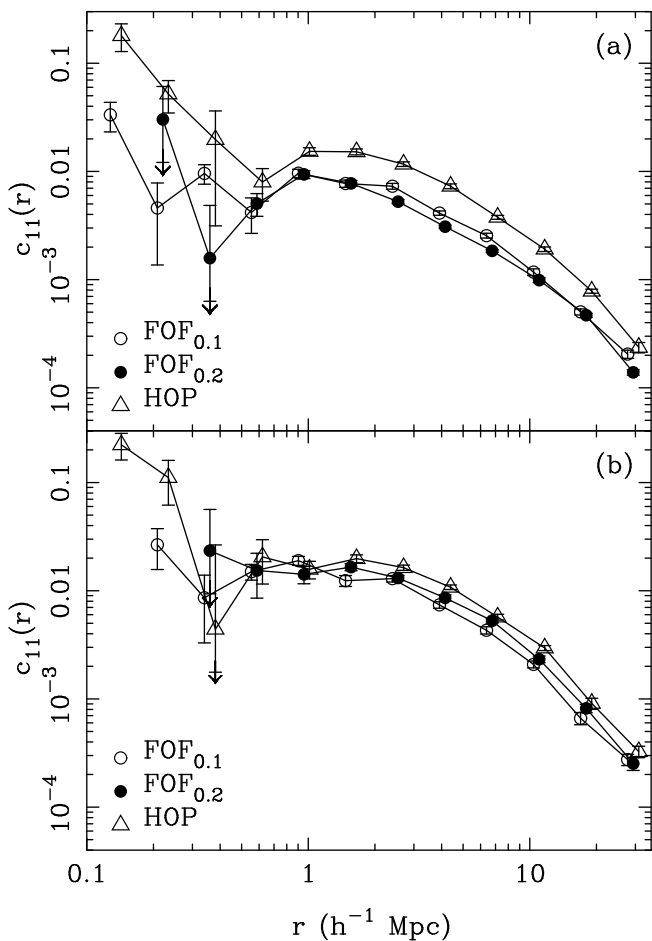


FIG. 3.— The ellipticity correlation function $c_{11}(r)$ (Equation 5) as a function of pair separation between halos in real space. In panel (a) we show results for all halos, for three different groupfinders (as in Fig. 1). In (b) we show results for halos of the same space density (we apply a minimum mass cut in each case and use the most massive 10000 halos in the simulation—see text). For clarity, the points have been displaced slightly in the x direction.

In general, these functions may be anisotropic, and depend on the separation between pairs both across and along the line of sight. We will plot their full dependence on these quantities later. In our tests of different halo finders and simulation resolution, we will work with $c_{11}(r)$ only (although we have checked that our conclusions are valid for the other functions also). This is because c_{11} has no strong angular dependence, so that plotting it as a solely a function of r does not hide any crucial aspects.

We show $c_{11}(r)$ in Fig. 3, for the three different groupfinders. In the top panel, we give results for all halos with > 20 member particles. The error bars are the equivalent of Poisson errors, calculated by randomly rotating the halo major axes and the calculating $c_{11}(r)$ for this randomized distribution (see e.g., VW). The dispersion between results for several such randomizations (we use 50) gives the error bar. In order to make best use of all the information contained in the simulation, we have averaged results from the three orthogonal projections of

the halo particles.

The first thing to notice is that there is a good detection of a signal, even for the largest bin that we plot. The widest pairs we use have a separation of 0.25 times the box side-length, or $35 h^{-1}\text{Mpc}$. This is not necessarily that surprising, given that large scale correlations in the matter distribution exist on such scales and beyond.

The $\text{FOF}_{0.1}$ and $\text{FOF}_{0.2}$ halos give very similar results. As mentioned earlier, this is a good test of the robustness of the correlation signal and a good argument that there are not systematic problems. It is telling us that the inner and outer parts of halos are responding in the same way, a stability which points to the correlation being a real effect. The HOP results are larger by a factor of ~ 2 , and on small scales seem to deviate even more. We have already seen from Fig. 1 that with the free parameters set in the way we have chosen, this groupfinder seems to produce groups which are clumps of subgroups which the FOF algorithm keeps separate. This is probably an indication that for a more reasonable result, we would need to tune some of the six free parameters that govern HOP.

Some of the differences between $c_{11}(r)$ results might be due to the fact that the same absolute mass cut (20 particles) for all three groupfinders will result in different halos being chosen. For example, the $\text{FOF}_{0.1}$ halos will be much rarer than $\text{FOF}_{0.2}$. A better way to compare results is to set the space density of halos to be equal. We have done this the bottom panel of Fig. 3, where we show $c_{11}(r)$ for the most massive 10000 halos in the simulation volume. The lower mass limits for the different groupfinders in this case are 44, 90 and 85 particles ($6.2 \times 10^{11} h^{-1} M_{\odot}$, $1.3 \times 10^{12} h^{-1} M_{\odot}$ and $1.2 \times 10^{12} h^{-1} M_{\odot}$), for $\text{FOF}_{0.1}$, $\text{FOF}_{0.2}$ and HOP, respectively. The results are indeed more similar now, except for the HOP results at the smallest separations. We have also tried applying an upper mass cut, keeping only halos containing less than a certain number of particles. We find similar results (not plotted) to those for all halos.

For the rest of the paper, we have decided to use groups chosen by the $\text{FOF}_{0.1}$ groupfinder. This is because we are most interested in the inner parts of halos, which is where galaxies will tend to lie. Also, when halos are chosen to have the same space density (Fig. 3b), these halos have a slightly lower correlation than the others, so that we are being conservative.

One can ask about the effect of simulation resolution on our results, whether the simulations have converged and if not, whether lower resolutions yield higher or lower correlations. In Figure 4, we compare halos taken from the larger, low resolution simulation ($240 h^{-1}\text{Mpc}$ boxsize) to our previous results. We again use the $\text{FOF}_{0.1}$ groupfinder, and in order to compare halos with the same mass, we use halos containing > 20 particles in the low resolution case and > 100 in the high resolution case (these halos do in fact have the same space density, indicating that the simulations have converged as far as the mass function is concerned).

We can see that although the ellipticity correlations have not converged, the higher resolution simulation is more correlated. This may be because structure has been allowed to form on smaller scales, whereas if the the structure is unresolved, some of the tidal field which causes correlations to arise is missing. In any case, we can argue

that the fact that higher resolution increases the correlated signal means that our results are likely to be conservative. Of course this situation is far from ideal, and one would really like to see if even higher resolution results do in fact converge. Such simulations are beyond the scope of this paper, however. This is particularly true because it is important not to sacrifice a cosmologically interesting volume for the sake of higher resolution, since long range tidal forces may play a significant role in setting up the correlations.

In Fig. 5, we show c_{11} and c_{22} as a function of halo pair separation across the line of sight (σ) and along the line of sight (π). This presentation is similar to that used in plotting redshift distortions of the matter correlation function (e.g., Kaiser 1987). Only $c_{22}(\sigma, \pi)$ appears to be severely anisotropic. The plot seems to be showing us that projected halos tilt in opposite directions (-ve correlation) when they are side-by-side, but in the same direction when they lie one behind the other. The $c_{11}(\sigma, \pi)$ function is nearly isotropic, and positive, so that pairs of halos have a tendency to stretch along the projection of the line joining them whatever their spatial orientation.

If c_{22} is measured averaged in radial bins, r (where $r = \sqrt{\sigma^2 + \pi^2}$) then the signal from the bottom right partly cancels that in the top left and the result is a very small correlation function. On the other hand, a projection of c_{22} on the plane of the sky (which we will do later when calculating the angular correlations) is equivalent to a projection along the π axis. Because π cannot be negative (it is defined as the modulus of the pair separation along the line of sight), then the contribution of the positive c_{22} signal at large π will result in a significant angular signal.

We do not plot the cross-correlation, $c_{12}(\sigma, \pi)$ here, as we find it to be consistent with zero everywhere. We also

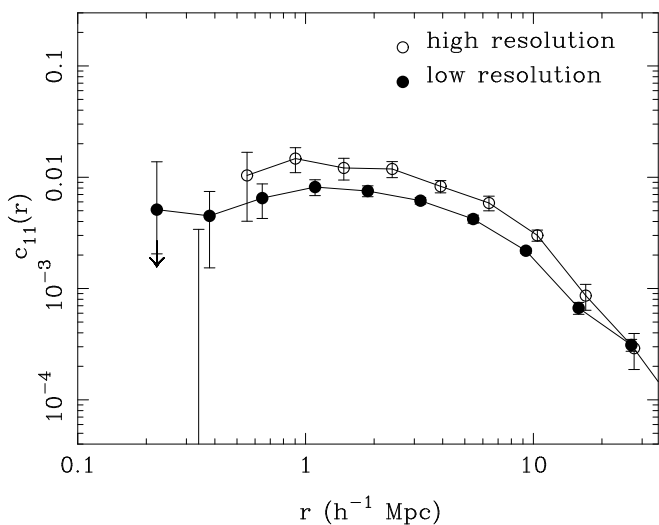


FIG. 4.— The ellipticity correlation function $c_{11}(r)$ (Equation 5) as a function of pair separation between halos in real space. We show results for halos of the same mass (which also have the same space density) taken from simulations with two different spatial and mass resolutions (see text). The lower resolution simulation is larger in volume by a factor ~ 5 , and has a mass resolution ~ 5 times lower. For this figure, and the rest of the paper, we use FOF_{0.1} halos.

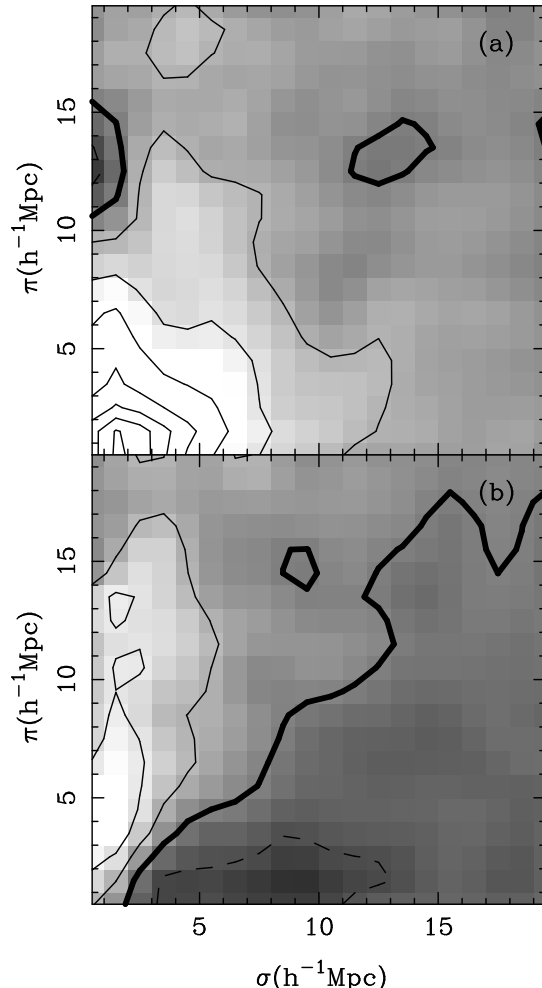


FIG. 5.— The ellipticity correlation functions, (a) $c_{11}(\sigma, \pi)$, and (b) $c_{22}(\sigma, \pi)$. Here σ is the distance between pairs of halos perpendicular to the line of sight, and π is the distance parallel to the line of sight. The values of c_{11} and c_{22} were originally binned into 20×20 bins in $\sigma \times \pi$. For clarity, we have plotted these results smoothed with a Gaussian window with dispersion $\sigma_w = 1$ bin. The contours represent increments of 0.001 in c_{11} and c_{22} , with the thickest contour representing 0 and dashed contours negative values.

note that in the observational case, plots like these (and the previous plots which were radially averaged) will be affected by redshift distortions of the pair separations.

4. SIMULATED SURVEYS

One way of making predictions for the ellipticity correlations that can be compared directly to current observations is by using simulated surveys with a similar geometry to real surveys. In this section we describe our creation of such datasets from the Nbody halo catalogs. In §5 we measure angular statistics from the simulated surveys and compare to analytic projection of the three dimensional statistics of §3.

The redshift distribution of faint background galaxies that are used in current weak lensing studies is not known accurately. Most of the observational groups assume that the peak of the redshift histogram lies around $z = 1$, so we will use this value in setting up our simulated surveys. We

note that depending on the actual redshift of the galaxies, the relative contribution and angular scale of the lensing correlations and any intrinsic correlation will vary, something which can undoubtedly be used to tell them apart. In our mock surveys, we will also assume that the galaxy population (we refer to halos as “galaxies” when describing the mock surveys) stays constant in comoving coordinates, so that we only make use of the $z = 1$ simulation output. We leave the study of the effects of redshift evolution to future work. Also, this approach will allow us to compare directly with the analytic projection of the statistics.

Following what has now become a standard technique (e.g., Jain, Seljak & White 2000, Croft et al. 2000) we stack simulation boxes one behind the other, from $z = 0$ to $z = 2$. Each simulation box is subjected to a random recentering, and possibility of reflection about one of the three centres. We place each with one of the three axes (randomly chosen) pointing along the line of sight. This procedure is adopted to avoid periodic repetition of structures. When projecting the box contents, we work in comoving coordinates, and set the angular size of the simulated catalog to be one box width at $z = 1$, where our z histogram will peak. At $z = 1$, an angular scale of 1 deg. therefore corresponds to $40 h^{-1}$ Mpc. We make use of the small angles involved by projecting onto a flat plane, rather than a curved sky. This facilitates things because the halo ellipticities have been defined in the same fashion.

The $N(z)$ form we choose for our mock surveys is a Gaussian distribution $N(z) = e^{(z-1)^2/(2\sigma_z^2)}$ (for simplicity’s sake), where we have centered on $z = 1$. We apply the selection function $\psi(r)$ which leads to such an $N(z)$ for a uniform distribution of galaxies, where $\psi(r)$ is the relative probability of including randomly chosen galaxy at a comoving distance r (see e.g., Peebles 1993). We try 3 values for σ_z , 0.4, 0.2 and 0.1. The widest of these is designed to mimic roughly the present observational catalogs which use no colour selection. The narrower redshift distributions could arise if some sort of photometric redshifts are used (narrower distributions still are possible, see e.g., Hogg et al. 1998).

It is necessary to project 26 box lengths to reach $z = 2$. For galaxies past the peak in the $N(z)$, the mock survey is wider than the simulation box. At this point we make use of the periodic boundaries and make each layer of boxes periodic across the line of sight. This was also done by e.g., Seljak, Burwell & Pen 2000) and should not cause any problems. In any case, we will compare with the analytic projection of the statistics to make sure.

We use only the FOF_{0.1} halos (with > 20 particles) to make our simulated surveys. This results in a rather small number of galaxies per square degree, ~ 18000 (for $\sigma_z = 0.4$), compared to e.g., $\sim 10^5$ for VW. The $N(z)$ for three surveys made using different value of σ_z is plotted in Fig. 6. We set the selection function to zero for $z < 0.3$ and $z > 2$.

In Fig. 7, we show the x and y components of the ellipticities on the plane of the sky, where we have binned the individual e_1 and e_2 values in square cells of side-length 2 arcmins. We plot as a line, the average ellipticity in each cell in a manner analogous to the individual halo ellipticities plotted in Fig. 1. We also show, as a grayscale, the angular area density of halos smoothed with a Gaussian

filter of FWHM 2 arcmins. Fig. 7a represents a survey with a wider z distribution ($\sigma_z = 0.4$) than Fig. 7b. The obvious difference between the two is that the wider distribution has washed out both the density inhomogeneities and the absolute value of the residual ellipticities. To the eye, there does not seem to be any obvious correlation between the ellipticity vectors, although as we will see in the next section, there are detectable statistical correlations and a non-zero shear variance. We defer any exploration of the relation between the projected halo density and ellipticities to future work.

5. ANGULAR STATISTICS

5.1. Angular ellipticity correlations

The ellipticity correlations measured in three dimensions in §3 can be projected for direct comparison with results from angular galaxy surveys. This can be done simply using a modification of Limber’s equation (Limber 1953, Peebles 1993), so that the angular correlation function of e_1 components of pairs is

$$C_{11}(\theta) = \frac{\int (r_1 r_2)^2 dr_1 dr_2 \psi_1 \psi_2 (1 + \xi(r_{12}) c_{11}(\sigma, \pi))}{[\int r^2 dr \psi]^2 + \int (r_1 r_2)^2 dr_1 dr_2 \psi_1 \psi_2 \xi(r_{12})}, \quad (8)$$

where r_{12} comoving is the separation between points at distance r_1 and r_2 from the observer. σ and π are the separations across and along the line of sight, which we calculate in the small angle limit, so that

$$\sigma = \left(\frac{r_1 + r_2}{2}\right)\theta, \quad \pi = |(r_1 - r_2)(1 - \theta^2/2)|, \quad (9)$$

and $r_{12} = \sqrt{\sigma^2 + \pi^2}$. The selection functions at r_1 and r_2 are given by ψ_1 and ψ_2 , and $\xi(r)$ is the halo autocorrelation function. The relations for the e_2 component correlation, $C_{22}(\theta)$ and the cross-correlation, $C_{12}(\theta)$ are analogous.

Using this formalism, we calculate $C_{11}(\theta)$, $C_{22}(\theta)$ and $C_{12}(\theta)$ for the three different selection functions also used

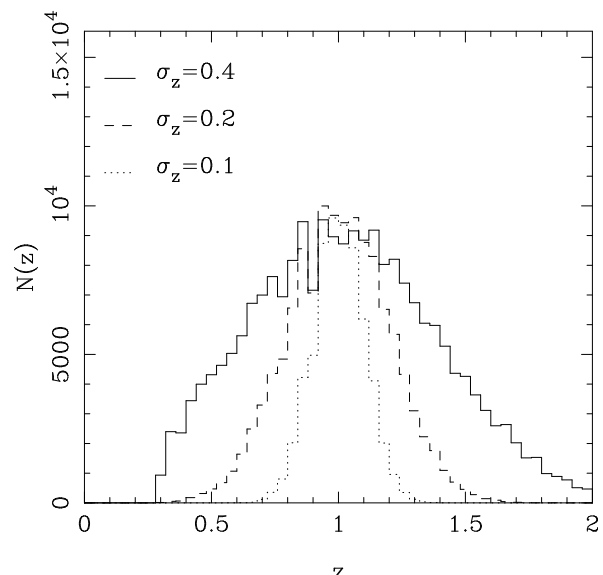


FIG. 6.— The actual redshift distribution of galaxies in simulated catalogs generated with different values of σ_z . We plot the number of galaxies in bins of width $\Delta_z = 0.04$

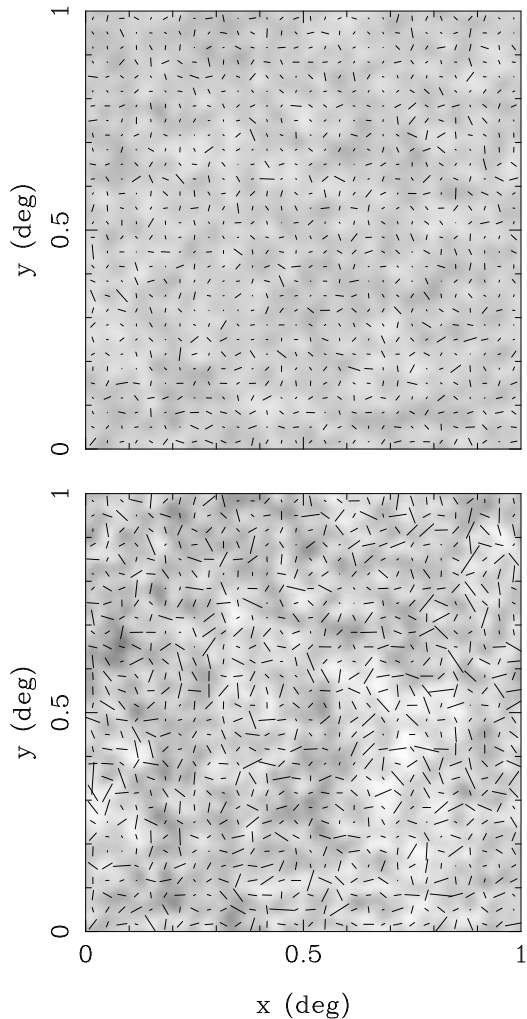


FIG. 7.— A 1 deg \times 1 deg patch of the simulated sky. 1 deg corresponds to a comoving size of $40 h^{-1}$ Mpc at $z = 1$, where the galaxy distribution peaks. The upper panel is for a survey where the galaxies have a wide redshift distribution ($\sigma_z = 0.4$), and the lower panel has $\sigma_z = 0.1$. We have show the ellipticities averaged in square bins of width 2 arcmin, as bars, with a length of 0.15 deg corresponding to an ellipticity of 1. We also show the projected halo density field smoothed with a Gaussian filter of FWHM 2 arcmin, with a linear grayscale.

in our simulated surveys, which yield a Gaussian $N(z)$. The results are plotted in Fig. 8. We can see that for the first two of these a distinct correlation signal results. The behaviour as a function of redshift width of the galaxy distribution is as we might predict, with a wider distribution yielding less angular correlation. Also very interesting is the fact that $C_{11}(\theta)$ is everywhere positive, whereas $C_{22}(\theta)$ dips below zero on the largest scales. The C_{12} function is much smaller, oscillating about zero, due to noise. These functional forms are very similar to the theoretical expectation for the weak lensing signal (see e.g., Miralda-Escudé 1991, Kaiser 1992). A simple explanation of this similarity is that the shear field which is responsible for the weak lensing correlations is mathematically similar to the shear field responsible for generating galaxy intrinsic shapes and spins from the surrounding large-scale structure, something which can be used to make fully analytic

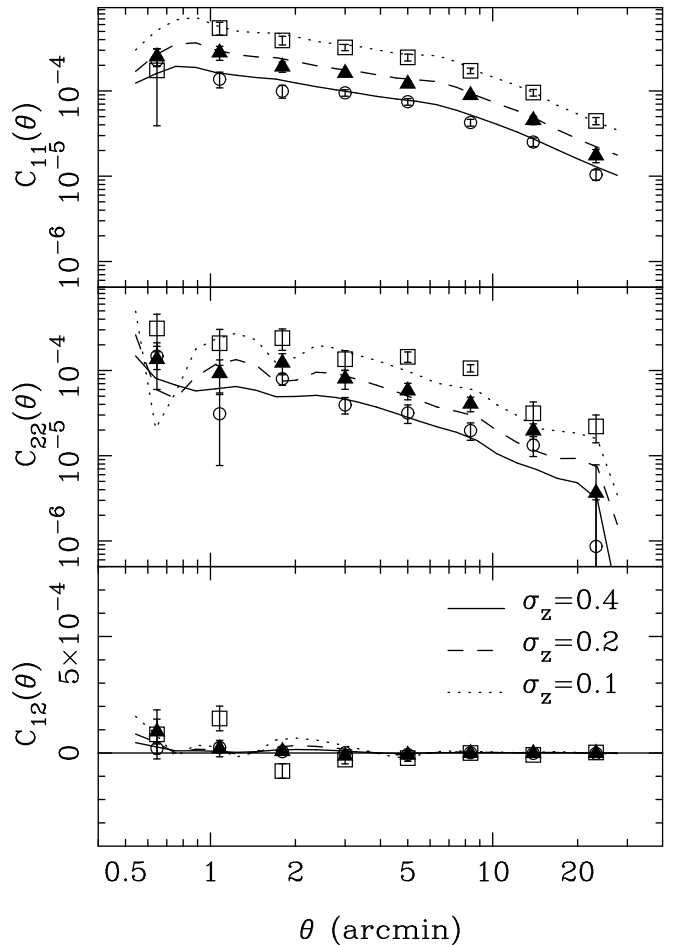


FIG. 8.— Comparison of angular ellipticity correlation functions computed using Equation 8 (lines) and directly from simulated catalogs (points). We show correlations of the e_1 components (C_{11}) the e_2 components (C_{22}) and the cross correlation of components (C_{12}), as a function of pair separation between halos in angular coordinates. Note that in the bottom panel, the y-axis is on a linear scale.

predictions of the effect, in the context of linear theory (Kamionkowski, private communication). We will return briefly to this in §7.

We have put points on Fig 8 which come from directly estimating the correlation functions from our simulated surveys of §4. We use as estimators the angular analogs of equations 5-7. The error bars have been computed from the error on the mean measured from 10 simulated surveys set up with different random seeds. As we use the same underlying Nbody simulation for all, this will result in an underestimate of the cosmic variance. This is adequate for our purposes, because we are comparing to the Limber's equation projection of the three dimensional statistics which is not likely to be exact anyway, as it involves numerical intergration of a noisy function. This is particularly true of $C_{22}(\sigma, \pi)$. That said, the agreement between the two sets of angular statistics is good, so that we can be fairly confident that there are no serious errors in the conversion of three dimensional statistics to angular ones.

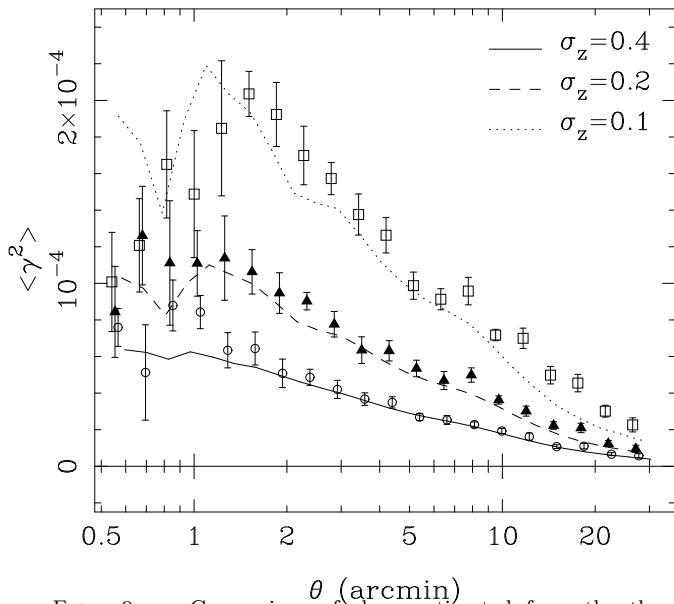


FIG. 9.— Comparison of shear estimated from the three-dimensional ellipticity correlation (Equations 8 and 11) and results measured directly from simulated angular surveys (see §5.2). We show results for three different redshift widths of the $N(z)$ distribution (see Fig.6).

5.2. Shear variance

The variance of the galaxy ellipticities binned into cells on the plane of the sky is a simple and interesting statistic to calculate. An estimator for the shear in a cell centred on angular position ϕ_i is (following VW, although note that we assume that the shear, $\gamma = \langle e \rangle / 2$, in the limit of intrinsically round galaxies, so that our definition is slightly different) is

$$E[\gamma^2(\phi_i)] = \left[\frac{1}{2N} \sum_{j=1}^N e_{1,j} \right]^2 + \left[\frac{1}{2N} \sum_{j=1}^N e_{2,j} \right]^2, \quad (10)$$

where there are N galaxies in the cell and $e_{1,j}$ and $e_{2,j}$ are the ellipticity components of the j th galaxy, which have been defined with respect to some fixed axes. The shear variance is then $\langle E[\gamma^2(\phi_i)] \rangle = (\sigma_e^2/4N) + \langle \gamma^2 \rangle$. Here $(\sigma_e^2/4N)$ is an ellipticity shot noise term, arising from the random intrinsic ellipticities of the finite number of galaxies involved, and $\langle \gamma^2 \rangle$ is the quantity we are interested in.

In terms of the angular ellipticity correlation functions, $\langle \gamma^2 \rangle$ is given by a double integral over the cell being used (as in the relation between ξ and counts-in-cells variance, e.g., Peebles 1993), so that

$$\langle \gamma^2 \rangle = \frac{1}{4A^2} \iint C_{11}(\theta) + C_{22}(\theta) d^2 A, \quad (11)$$

where A is the cell area. We note that this integral will tend to be dominated by the largest θ scale, so that sensitivity to systematic errors on small scales will be relatively low.

We carry out this integration using our angular ellipticity correlations from Fig. 8. For easy comparison with our simulated survey results (see below), we use square cells of side length L . In Figure 9, we show the $\langle \gamma^2 \rangle$ curves that result from the integral, as a function of angular scale

$\theta = L/\sqrt{\pi}$. This x -axis scaling was chosen because some observational groups (e.g., VW) calculate $\langle \gamma^2 \rangle$ in round cells of radius θ .

From the plot, we can see that $\langle \gamma^2 \rangle$ rises as we move from large to small scales. The rms shear, $\langle \gamma^2 \rangle^{1/2}$ at $\theta = 2$ arcmins is $\sim 0.6\%$ for a wide redshift distribution ($\sigma_z = 0.4$). This is significantly below the theoretical prediction for the rms shear due to weak lensing in different cosmological models, which can vary from $\sim 1\%$ to $> 3\%$ (see e.g., VW). Because the contributions to this quantity add in quadrature, the intrinsic shear is likely only to matter for low amplitude models. Of course, as we have only simulated one (relatively high amplitude) model, it could be that the intrinsic shear for low amplitude cosmologies is also lower. For a narrower redshift distribution with $\sigma_z = 0.1$, our value of $\langle \gamma^2 \rangle^{1/2}$ doubles. On large scales we also see that there is still signal out to $\theta = 30$ arcmins.

For comparison, we again show points representing the value of $\langle \gamma^2 \rangle$ measured from the simulated surveys. We have used the estimator of equation 10, with square cells of side length $L (= \sqrt{\pi}\theta)$. To remove the shot noise term, we use the procedure advocated by VW. This involves randomly rotating the major axes of all the projected halos and calculating $\langle \gamma^2 \rangle$, which will be a noisy version of the shot noise term. We carry out 1000 such randomizations and use the average $\langle \gamma^2 \rangle$ measured from them as our $\sigma_e^2/4N$, which we subtract. The results are shown in Fig. 9, with error bars which are again the error on the mean from 10 simulated surveys. As with the ellipticity correlation functions, the agreement is good.

6. COMPARISON WITH OBSERVATIONS

As mentioned in §1, there are now several different groups (VW; Bacon, Refregier & Ellis 2000; Wittman et al. 2000; KWL) producing results from large observational campaigns to measure weak lensing by large-scale structure. These different surveys (at the time the published results were submitted) involved from 0.5 to 1.8 square degrees of imaging data, and produced measurements of ellipticity correlations and shear on scales from ~ 0.6 to ~ 30 arcmins. In this section, we will briefly compare these current measurements with the predictions of §5.

Two of these groups (VW, and Wittman et al. 2000) and have published ellipticity correlation functions, using slightly different notation from ours. What we call $C_{11}(\theta)$, $C_{22}(\theta)$, are called $\langle e_t(0)e_t(\theta) \rangle$, $\langle e_r(0)e_r(\theta) \rangle$ by VW, and $\langle e_1e_1 \rangle$, $\langle e_2e_2 \rangle$ by Wittman et al. (2000). The cross correlation $C_{12}(\theta)$ is defined analogously.

We show these observational results in Fig. 10, together with those from the simulated surveys (from Fig. 8). The measurements from the two groups are mostly at different scales, but agree within the errors in the small degree of overlap around $\theta = 3.5$ arcmins. The functional form of our intrinsic correlation follows roughly the observational results. The amplitude is however much lower, by a factor of roughly between 5 and 10 for most of the points, for the most relevant redshift distribution (a wide one, with $\sigma_z = 0.4$). The Wittman et al. points appear to be even higher than this on large scales for C_{22} . We note that in the Wittmann et al. paper, these points are shown to also be rather higher compared to theoretical weak lensing predictions for Λ CDM than the C_{11} points. For a narrower

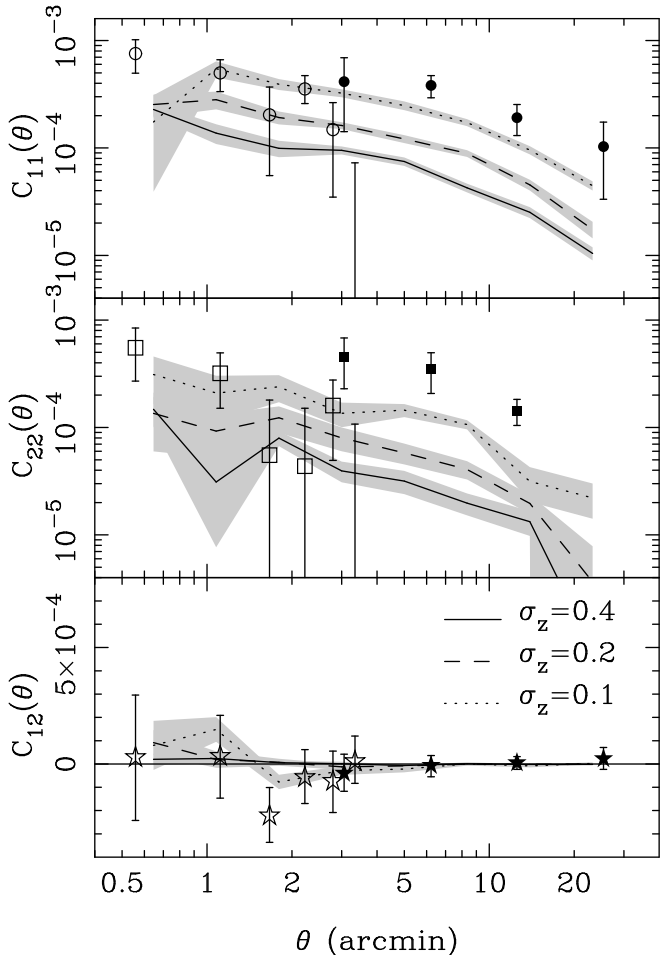


FIG. 10.— The angular ellipticity correlation functions measured from galaxy survey data by VW (open symbols) and Wittman et al. (2000) (filled symbols). We also show the measurements made in §5 from our simulated surveys, for three different values of the redshift width (σ_z). The value of σ_z which is likely to be closest to that in the observed galaxy distributions is $\sigma_z = 0.4$, which gives the lowest curves. We show the error bars taken from Fig. 8 as shaded regions.

redshift distribution, which may be achieved in the future with photometric redshifts, the intrinsic correlations are closer to the current observational data. The cross correlation, C_{12} , while noisy, is small, and consistent with zero in all cases.

If we move to the shear variance, $\langle \gamma^2 \rangle$, we can plot results from all four groups. We have the plotted these in the same format as Figure 2 of KWL, as Fig. 11. As Wittman et al. did not specifically publish $\langle \gamma^2 \rangle$ values, we have converted their C_{11} measurements using the formulae in Kaiser (1992) (as was done in KWL, to which the reader is referred for details), assuming a spectral index of mass fluctuations of $n = -1$. One difference between this plot and that in KWL is that we plot the results as a function of θ , the radius of a top-hat sphere. To do this, we have converted the square box side-length L from KWL to the radius of a circle with the same area ($\theta = L/\sqrt{\pi}$; this is the same as was done in plotting Fig. 8). The groups all have results which appear to be consistent within their errors, which is impressive and reassuring.

Turning to the simulation results, we concentrate first

on the wide redshift distribution ($\sigma_z = 0.4$), which is most relevant to the current observations. The intrinsic $\langle \gamma^2 \rangle$ we predict is a small fraction of the measured value on all scales, except possibly for the largest scale point from KWL, which, as those authors point out is an interesting null detection. The intrinsic $\langle \gamma^2 \rangle$ is also at a smaller level than the 1σ errors for the observational measurements. It is therefore not really a factor when interpreting the current results, but may become a bit more of an issue when the surveyed areas increase and the statistical errors become smaller. If we now turn to the other two curves, we can see that for the narrow redshift distributions, the intrinsic $\langle \gamma^2 \rangle$ begins to approach the current measurements, at least on large scales. On small scales, although the errors are large (Fig. 9), there appears to be relatively less signal.

7. SUMMARY AND DISCUSSION

We have used Nbody simulations to make predictions for intrinsic correlations of galaxy ellipticities, under the assumption that galaxy shapes follow the shapes of their dark matter halos. Measurements of the ellipticity correlation functions in three-dimensions give a distinctive signal, which we measure with relatively small uncertainties on scales from $\sim 0.5 - 30 h^{-1}$ Mpc. These correlations vary by less than a factor of ~ 2 for different halo finding techniques and different simulation resolutions. We project these three dimensional correlations into angular statistics, including the shear variance. We have done this both analytically, using a modified Limber's equation, and by making direct measurements from simulated surveys constructed by projecting the simulation boxes. We find that the amplitude of the angular statistics depends strongly on the redshift width of the galaxy distribution. With widths appropriate to present day surveys, we find that the in-

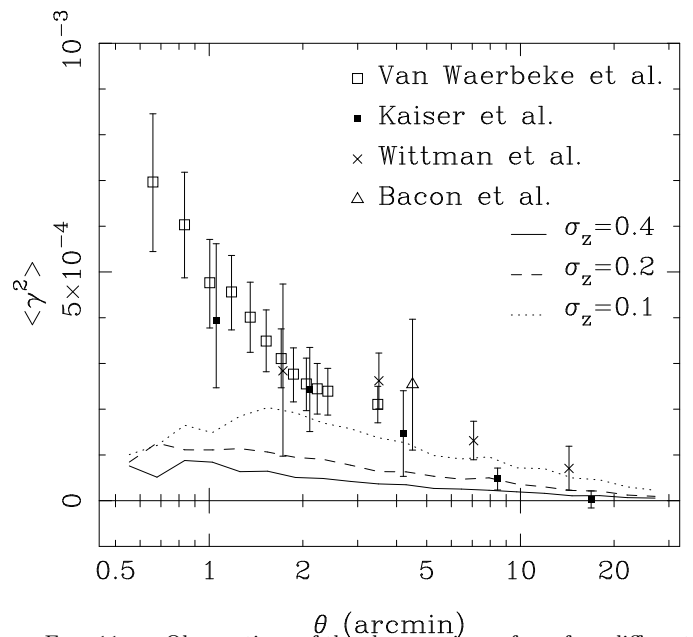


FIG. 11.— Observations of the shear variance from four different groups (points with error bars), together with results from our simulated surveys (lines). We show the latter for three different values of the redshift width (σ_z). The value of σ_z which is likely to be closest to that in the observed galaxy distributions is $\sigma_z = 0.4$, which gives the lowest curves. The error bars on the simulation points can be obtained from Fig. 9.

trinsic correlations we predict are around 10 – 20% of the currently measured signal, somewhat smaller than the 1σ errors on the measurements.

Since the area of the sky surveyed for weak lensing is increasing rapidly, the intrinsic correlation may become detectable from these deep and wide surveys in the future. In any case, it seems to be worth bearing in mind that there could be this sort of contamination. In particular, one possible way of extracting more information from lensing which has received attention is the use of photometric redshift information, to break down the background galaxy distribution into a number of “screens”. This would enable tomography to be carried out (e.g., Hu 1999). We have seen however that the intrinsic correlation may be quite large for these narrow redshift bins, so that it might become comparable to the weak lensing signal (Fig. 11).

Of course, the extra information available in the form of photometric redshifts is likely to be very useful for deciding whether there is an intrinsic component, and if it exists, to separate it from the lensing signal. For example the cross-correlation of ellipticities (or co-variance of the shear) between different redshift bins can be compared to the correlation within bins, with only the later responding to intrinsic correlations. Something along these lines has already been carried out by KWL, albeit with two colour bands which both give wide redshift distributions (but with one deeper than the other). These authors find a higher shear signal for the deeper redshift sample, which is consistent with lensing, but in the wrong direction for intrinsic correlations. For the cross-correlation between samples, they do find slightly anomalous results, however.

Another way of trying to measure any intrinsic ellipticity correlations would be to stick to the local universe, and to measure the three dimensional correlation functions (§3) from a redshift survey. If there really is a signal like that plotted in Fig. 3, then this could be measurable from a relatively small survey (by today's standards), with a few thousand galaxies. Even without redshifts, one might expect to find a measurable intrinsic signal from a relatively nearby angular sample of galaxies, like the APM survey (Maddox et al. 1990), or Sloan Digital Sky Survey (Gunn & Weinberg 1995).

If there are in fact some measurable correlations between real galaxy ellipticities, then this can be understood in the framework of structure formation by gravitational instability, with the ellipticities being linked to the angular momenta of galaxies, which are in turn set up by tidal torques from the shear in the initial density field (e.g., Peebles 1969, Barnes & Efstathiou 1987, Catelan and Theuns 1996a,b). This may explain why the ellipticity correlation functions we measure have similar functional forms to those caused by weak-lensing: both are responding to a cosmic shear field. Detection of correlated ellipticities, if they exist, may be useful for the study of galaxy formation (e.g., Sugerman et al. 2000), or even cosmology (Lee & Pen 2000).

It is also likely that the signal due to the intrinsic correlation will give qualitatively and measurably different results from weak lensing for some statistics we have not considered here. For example, the probability distribution of the lensing convergence is predicted to have a measurable skewness, something which can be used to determine Ω (Bernardeau et al. 1997). Measurements of this param-

eter from our simulated surveys by L. Van Waerbeke (private communication) yield a null result, the convergence pdf being consistent with a Gaussian distribution. The intrinsic correlations do not therefore appear to interfere with our ability to do cosmology in this way, and should not act as more than an additional source of noise (albeit correlated) when reconstructed mass maps are made.

On the simulation side, one important issue is the fact that our results have apparently not converged with resolution. Although we find that the higher resolution of two simulations gives more intrinsic correlations, it is possible that given even higher resolution, things will begin to go the other way. Clearly this needs to be tested somehow in the future. Also, perhaps most important of all, we have assumed a very simple relationship between projected halo ellipticities and projected galaxy ellipticities. It is possible that adding gas dynamics and star formation to simulations will result in their being no significant correlation between the two. The tests which we have carried out which have most bearing on this are the use of two sets of different friends of friends groups, which respond to ellipticities either of the whole halo, or just the dense central region. As we find results for the two which are very similar, this is at least some evidence that the intrinsic correlation may be fundamental.

As this paper was being completed, we became aware of similar work by Heavens et al. (2000). These authors use the angular momentum of Nbody halos (also from Virgo simulations, but only at the lower of the two resolutions) to predict the intrinsic correlation of spiral galaxy ellipticities. They reach final results which are broadly similar (although they find much more noise), and also conclude that while these effects are likely to be minor for present surveys, they may become important with small redshift widths (in their case for shallower surveys). We also became aware of analytic work on a similar theme by Catelan et al. (in preparation), and Mackey and White (in preparation).

We thank Ludo Van Waerbeke, Martin White, Volker Springel, Marc Kamionkowski, and Jordi Miralda-Escudé for useful discussions, and Nick Kaiser for help in interpreting some observational results. We also thank George Efstathiou for supplying us with the FOF groupfinder and the Virgo consortium for making their simulation data public. RACC acknowledges support from NASA Astrophysical Theory Grant NAG5-3820.

REFERENCES

- Argyres, P.C., Groth, E.J., Peebles, P.J.E., & Struble, M.F. 1986, *AJ*, **91**, 471.
- Bacon, D., Refregier, A., & Ellis, R. 2000, *MNRAS*, submitted.
- Barnes & Efstathiou, G., 1987, *ApJ*, **319**, 575.
- Bernardeau, F., Van Waerbeke, L., & Mellier, Y. 1997, *A&A*, **322**, 1.
- Binggeli, B. 1982, *A&A*, **107**, 338.
- Blandford, R.D., Saust, A.B., Brainerd, T.G., & Villumsen, J.V. 1991, *MNRAS*, **251**, 600.
- Cabanela, J.E., & Dickey, J.M. 1999, *AJ*, **103**, 393.
- Catelan, P., & Theuns, T. 1996a, *MNRAS*, **282**, 436.
- Catelan, P., & Theuns, T. 1996b, *MNRAS*, **282**, 455.

- Catelan, P., & Theuns, T. 1997, *MNRAS*, **292**, 225.
- Ciotti, L., and Dutta, S.N. 1994, *MNRAS*, **270**, 390.
- Coutts, A. 1996, *MNRAS*, **278**, 87.
- Croft, R.A.C., Davé, R., Hernquist, L., & Katz, N., 2000, *ApJ*, in press, astro-ph/0002422
- Couchman, H.M.P., Thomas, P.A., and Pearce, F.R., 1995, *ApJ*, **452**, 797
- Davis, M., Efstathiou, G., Frenk, C. S., White, S. D. M., 1985, *ApJ*, **292**, 371
- Dekel, A., West, M.J., & Aarseth, S.J. 1984, *ApJ*, **279**, 1.
- isenstein, D.J., Hut, P., 1998, *ApJ*, **498**, 137
- Flin, P. 1987, *MNRAS*, **228**, 941.
- Flin, P. 1988, *MNRAS*, **235**, 857.
- Fong, R., Stevenson, P.R.F., & Shanks, T. 1990, *MNRAS*, **242**, 146.
- Garrido, J.L., Battaner, E., Sánchez-Saavedra, M.L., & Florido, E. 1993, *A&A*, **271**, 84.
- Gunn, J.E., and Weinberg, D.H., 1995, in *Wide Field Spectroscopy and the Distant Universe*, ed. Maddox, S., & Aragón-Salamanca, A. (Singapore: World Scientific), 3
- van Haarlem, M., & van de Weygaert, R. 1993, *ApJ*, **418**, 544.
- Heavens, A., Refregier, A., and Heymans, C., 2000, *MNRAS*, submitted, astro-ph/0005269
- Hogg, D.W., et al. , 1998, *AJ*, **115**, 1418.
- Hu, W., 1999, *ApJ*, **522**, L21.
- Jain, B., & Seljak, U. 1997, *ApJ*, **484**, 560.
- Jain, B., Seljak, U., & White, S., 2000, *ApJ*, **530**, 547
- Jenkins, A., Frenk, C. S., Pearce, F. R., Thomas, P. A., Colberg, J. M., White, S. D. M., Couchman, H. M. P., Peacock, J. A., Efstathiou, G., Nelson, A. H., 1998, *ApJ*, **499**, 20
- Kauffmann, G., Colberg, J.M., Diaferio, A., White, S.D.M., 1999, *MNRAS*, **303**, 188.
- Kaiser, N. 1987, *MNRAS*, **227**, 1
- Kaiser, N. 1992, *ApJ*, **388**, 272.
- Kaiser, N., Wilson, G., & Luppino, G.A. 2000, *ApJ*, submitted.
- Lambas, D.G., Groth, E.J., & Peebles, P.J.E. 1988, *AJ*, **95**, 996.
- Lambas, D.G., Nicotra, M., Muriel, H., & Ruiz, L. 1990, *AJ*, **100**, 1006.
- Lee, J., and Pen, U. 2000, *ApJ*, **532**, 5.
- Limber, D.N., 1953, *ApJ*, **117**, 134.
- Maddox, S., Efstathiou, G., Sutherland, W.J., Loveday, J., 1990, *MNRAS*, **243**, 692.
- Miralda-Escudé, J. 1991, *ApJ*, **380**, 1.
- Muriel, H., & Lambas, D.G. 1989, *AJ*, **98**, 1995.
- Muriel, H., & Lambas, D.G. 1992, *AJ*, **103**, 393.
- Peebles, P.J.E., 1969, *ApJ*, **155**, 393.
- Peebles, P.J.E., 1993, *Principle of Physical Cosmology*, (Princeton: Princeton University Press)
- Plionis, M. 1994, *ApJS*, **95**, 401.
- Rhee, G., van Haarlem, M., & Katgert, P. 1992, *AJ*, **103**, 1721.
- Seljak, U., Burwell, J., & Pen, U-L., 2000, *Phys. Rev. D*, submitted, astro-ph/0001120
- Splinter, R.J., Melott, A.L., Linn, A.M., Buck, C., and Tinker, J. 1997, *ApJ*, **479**, 632.
- Struble, M.F., & Peebles, P.J.E. 1985, *AJ*, **90**, 582.
- Sugerman, B., Summers, F.J., & Kamionkowski, M. 1999, *MNRAS*, **311**, 762 .
- de Theije, P.A.M., van Kampen, E., & Slijkhuis, R.G. 1998, *MNRAS*, **297**, 195.
- Ulmer, M.P., McMillan, S.L.W., & Kowalski, M.P. 1989, *ApJ*, **338**, 711.
- Van Waerbeke, L., Mellier, Y., Erben, T., Cuillandre, J.C., Bernardeau, F., Maoli, R., Bertin, E., Mc Cracken, H.J., Le Fèvre, O., Fort, B., Dantel-Fort, M., Jain, B., Schneider, P., 2000, *A&A*, in press.
- West, M.J. 1989a, *ApJ*, **344**, 535.
- West, M.J. 1989b, *ApJ*, **347**, 610.
- West, M.J., Dekel, A., & Oemler, A. 1989, *ApJ*, **336**, 46.
- West, M.J., Villumsen, J., & Dekel, A. 1991, *ApJ*, **369**, 287.
- Wittman, D.M., Tyson, J.A., Kirkman, D., Dell'Antonio, I., & Bernstein, G. 2000, *Nature*, in press.